Elsevier Editorial System(tm) for Science of the Total Environment
Manuscript Draft

Manuscript Number:

Title: Current and future assessment of soil erosion by water on the Tibetan Plateau

Article Type: Research Paper

Keywords: soil erosion by water; Tibetan Plateau; climate change; RUSLE; future erosion

Corresponding Author: Miss Hongfen Teng, Ph.D

Corresponding Author's Institution: zhejiang university

First Author: Hongfen Teng, Ph.D

Order of Authors: Hongfen Teng, Ph.D; Zongzheng Liang; Yong Liu; Raphael Viscarra Rossel; Adrian Chappell; Wu Yu; Zhou Shi

Abstract: Soil erosion by water is accelerated by warming climate, and negatively impacts food and water security and ecological conservation. The Tibetan Plateau (TP) has experienced warming at approximately twice the rate observed globally, and heavy precipitation events lead to an increased risk of erosion. Here, the Revised Universal Soil Equation (RUSLE) was performed to assess current (2002-2016) erosion on the TP and then predicted the potential for soil erosion by water in 2050. We used publicly available data and the most recent earth observation to derive our estimates at 1 km. To predict the soil loss in 2050, we first built a multiple linear regression (MLR) with the current rainfall erosivity data and a set of climatic and other covariates. Second, we generalised the coefficients of the MLR with climate covariates for 2050 derived from two representative concentration pathways (RCPs) and six global climate models (GCMs). Then, the soil erosion by water in 2050 was predicted by rainfall erosivity in 2050 and other erosion factors. The results show that the mean annual soil erosion rate on the TP under current conditions is 8.34 t ha-1 y-1, which is equivalent to an annual soil loss of 1,604×106 tonnes. Our 2050 projections suggested that erosion on the TP will increase to 9.73 t ha-1 y-1 and 11.60 t ha-1 y-1 under conditions represented by RCP2.6 and RCP8.5, respectively. The current assessment and future predicted soil erosion by water in the TP should be valuable for environment protection and soil conservation in this unique region and elsewhere.

Suggested Reviewers: Dominique Arrovays
INRA, Unité Infosol, 45075 Orléans, France
dominique.arrouays@inra.fr

Asim Biswas
School of Environmental Sciences, University of Guelph
biswas@uoguelph.ca

Thorsten Behrens
Institute of Geography, Physical Geography, University of Tübingen

thorsten.behrens@uni-tuebingen.de

A-xing Zhu
Department of Geography, University of Wisconsin
azhu@wisc.edu

Ganlin Zhang
Institute of Soil Science, Chinese Academy of Sciences
glzhang@issas.ac.cn

Opposed Reviewers:

2 Dec 2017

Attn: Editor Science of the Total Environment

Dear Editor,

My co-author and I would be grateful if you consider this manuscript for publication in *Science of the Total Environment*

'Current and future assessment of soil erosion by water on the Tibetan Plateau' by Teng et al.

The paper falls well within the scope of the journal because it addresses two challenges: first, to predict the current present soil erosion by water in the Tibetan Plateau using the Revised Universal Soil Loss Equation (RUSLE) and second, to predict the potential soil erosion in the year 2050 with climate projections from CMIP5 GCMs.

Our paper is novel and demonstrates that the average rate of soil erosion by water on the Tibetan Plateau under current conditions is 8.34 t ha^{-1} y^{-1}, which is equivalent to an annual total soil loss of $1{,}604\times10^{6}$ tonnes. Our 2050 projections suggested that erosion on the Tibetan Plateau will increase to 9.73 t ha^{-1} y^{-1} and 11.60 t ha^{-1} y^{-1} under conditions represented by RCP 2.6 and 8.5, respectively.

My co-authors and I all provided substantial contributions to the design, conduct, interpretation and writing of the manuscript. Our manuscript has been thoroughly revised and we have approval for submitting this final version to Science of the Total Environment.

We declare that the submitted work is our own and that copyright has not been breached in seeking its publication. We also declare that the submitted work has not previously been published in full, and is not being considered for publication elsewhere.

I hope that you will find the manuscript interesting and suitable for Science of the Total Environment. I look forward to your news.

Yours sincerely,

Professor Zhou **Shi**
Institute of Applied Remote Sensing and Information Technology

College of Environmental and Resource Sciences
Zhejiang University
310058, Hangzhou, China
Tel: +86 15168307951
Email: shizhou@zju.edu.cn

*Title Page

Current and future assessment of soil erosion by water on the Tibetan Plateau

Hongfeng Teng [1], Zongzheng Liang [1], Songchao Chen [2], Yong Liu [1], Raphael A. Viscarra Rossel[3], Adrian Chappell[4], Wu Yu [5], Zhou Shi [1*]

[1] College of Environmental and Resource Sciences, Zhejiang University, Hangzhou 310058, China;

[2] UMR SAS, INRA, Agrocampus Ouest, Rennes,35042, France;

[3] Bruce E. Butler Laboratory, Land & Water Flagship CSIRO, PO Box 1666, Canberra, ACT 2601, Australia;

[4] School of Earth and Ocean Science, Cardiff University, Cardiff CF10 3XQ, UK;

[5] College of Resource and Environment, Tibet University, Nyingchi, 860114, China

*Correspondence: e-mail: shizhou@zju.edu.cn; Tel.: +86-571-88982831

*Graphical Abstract

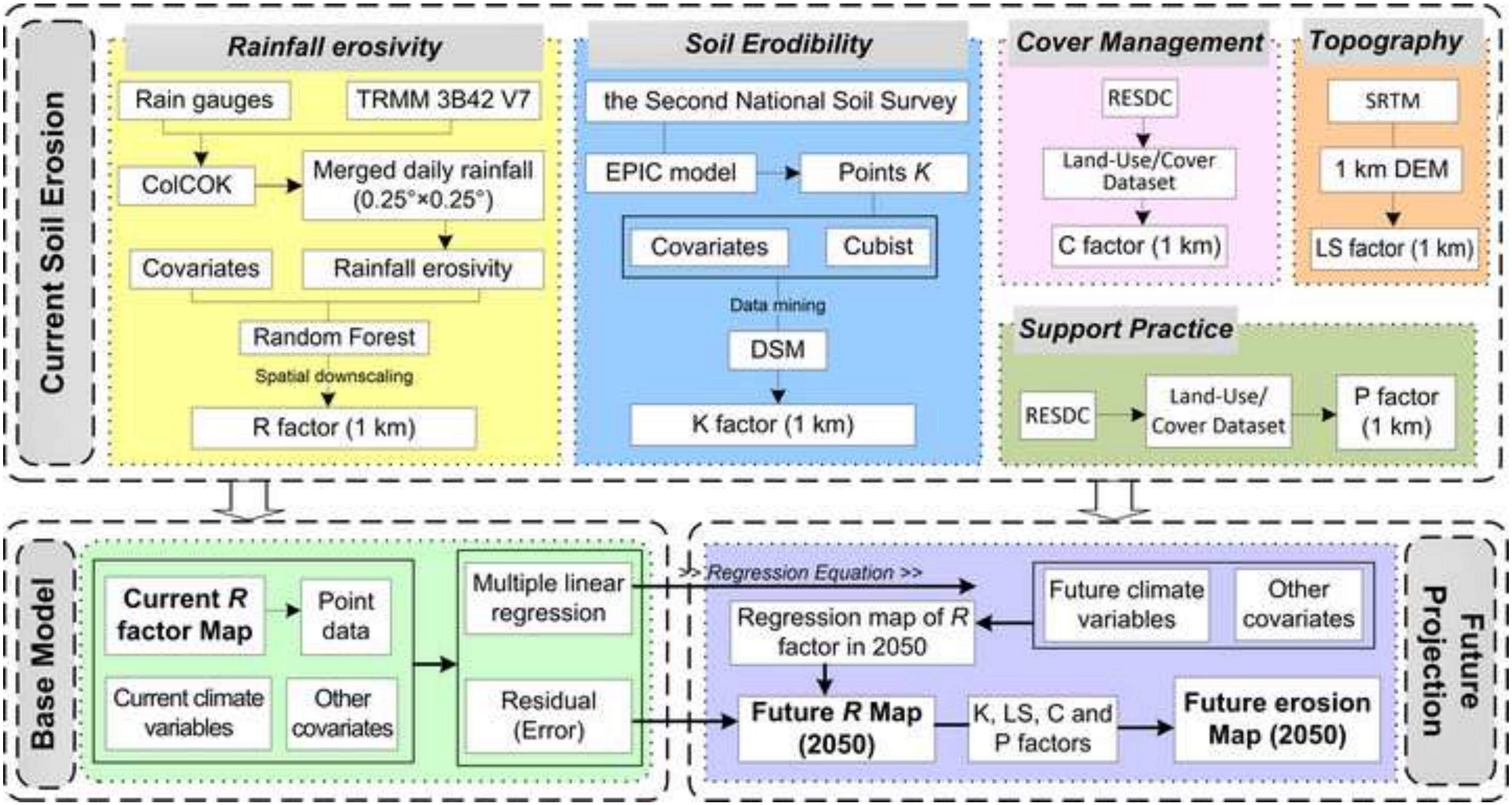

***Highlights (for review : 3 to 5 bullet points (maximum 85 characters including spaces per bullet point)**

- Present soil erosion by water on the Tibetan Plateau was predicted by RUSLE based on the most current and available data sets.
- Two RCPs and six GCMs were used to evaluate the climate change on the Plateau and were incorporated into the prediction of *R* factor in 2050.
- Soil erosion rate in 2050 was estimated with the corresponding projected *R* factor in 2050 and other erosion factors.
- The results suggest an overall increase of erosion rates in 2050 over the Plateau.

Current and future assessment of soil erosion by water on the Tibetan Plateau

Abstract

Soil erosion by water is accelerated by warming climate, and negatively impacts food and water security and ecological conservation. The Tibetan Plateau (TP) has experienced warming at approximately twice the rate observed globally, and heavy precipitation events lead to an increased risk of erosion. Here, the Revised Universal Soil Equation (RUSLE) was performed to assess current (2002–2016) erosion on the TP and then predicted the potential for soil erosion by water in 2050. We used publicly available data and the most recent earth observation to derive our estimates at 1 km. To predict the soil loss in 2050, we first built a multiple linear regression (MLR) with the current rainfall erosivity data and a set of climatic and other covariates. Second, we generalised the coefficients of the MLR with climate covariates for 2050 derived from two representative concentration pathways (RCPs) and six global climate models (GCMs). Then, the soil erosion by water in 2050 was predicted by rainfall erosivity in 2050 and other erosion factors. The results show that the mean annual soil erosion rate on the TP under current conditions is 8.34 t ha^{-1} y^{-1}, which is equivalent to an annual soil loss of $1{,}604\times10^{6}$ tonnes. Our 2050 projections suggested that erosion on the TP will increase to 9.73 t ha^{-1} y^{-1} and 11.60 t ha^{-1} y^{-1} under conditions represented by RCP2.6 and RCP8.5, respectively. The current assessment and future predicted soil erosion by water in the TP should be valuable for environment protection and soil conservation in this unique region and elsewhere.

Keywords: soil erosion by water; Tibetan Plateau; climate change; RUSLE; future erosion

1. Introduction

Soil erosion by water has become one of the greatest global threats to the environment (Chappell et al., 2016; Navarro-Hevia et al., 2016). With soil erosion by water, soil condition, water quality, species habitats and the provision of ecosystem services are negatively affected (Amundson et al., 2015; Teng et al., 2016). It is important to quantify the impacts of soil erosion by water and to develop effective measures for soil and water conservation. Soil erosion models are often employed to assess the risk of soil loss (Karydas et al., 2014). Among them, the Revised Universal Soil Loss Equation (RUSLE; Renard et al., 1997) has been applied commonly to estimates long-term soil erosion rate from hillslope in large scale studies (Panagos et al., 2015; Teng et al., 2016).

The effects of climate change on soil erosion by water have been described by researchers (Garcia-Fayos and Bochet, 2009; Li and Fang, 2016; Yang et al., 2003). The characteristics of rainfall (rainfall amount, intensity and spatio-temporal distribution) directly affect soil erosion. In addition, the rising temperature also indirectly affect soil erosion (Li and Fang, 2016). According to the Fifth Assessment Report (AR5) of the IPCC (Intergovernmental Panel on Climate Change) reports, the global mean precipitation and surface temperature have been have changed significantly, and suggests that these changes are very likely to continue in the 21st Century (IPCC, 2014). These effects still uncertain; therefore, the magnitude of the effects of climate variability on soil erosion needs to be investigated.

The Tibetan Plateau (TP), which is often known as “the Third Pole” of the Earth

(Qiu, 2008), has an average elevation of more than 4000 meter above sea level. Regional and global climate change have effects on the TP thorough thermal and mechanical forcing mechanisms (Su et al., 2013). The TP, which is also known as the "Asian water tower" (Immerzeel et al., 2010), is the source of the major river systems, and proved water to more than 1.4 billion people (over 20% of the global population). The soil erosion by water in the upstream areas will impact the water quality and food security in the downstream areas. Thus, the TP is of immense importance to both the climate and the ecosystems of Asia and the world, and more attention should be paid to the erosion status over these regions (Du et al., 2004).

The TP appears to be particularly sensitive to variations in climate and has become one of the most degraded ecosystems in the world (Baumann et al., 2009). In the 21st century, a warming trend of 0.47°C $(10\ yr)^{-1}$ to 0.73°C $(10\ yr)^{-1}$ over the TP under the representative concentration pathway 8.5 (RCP8.5) scenario has been predicted by the Global climate models from the fifth phase of the Coupled Model Intercomparison Project (CMIP5) (Su et al., 2013). Research of soil erosion by water in the TP may provide one of the last remaining chances to study the impact of climate change on water erosion over a large region because many of the natural ecological processes and feedbacks still intact in these areas (Chen et al., 2013). However, erosion prediction and risk assessment over the TP is great challenge, particularly if associated with climate change.

The soil erosion by water in the TP has been estimated by several scientists, but these are mostly focused on catchment (Chaplot et al., 2005; Hren et al., 2007; Jiang and Zhang, 2016) or local scale (Pan et al., 2010; Wang et al., 2014; Xu et al., 2009). Due to the high altitude, harsh weather conditions, and remoteness of the Plateau, the quantitative and direct measurements of water erosion over the TP are difficult, expensive, time-consuming and almost impossible. There is limited knowledge about the quantitative erosion rates over the whole TP. The lack of field measurement creates a need to develop new methods to predict soil erosion by water and the impacts of future climate change on erosion in this area. Modelling current and future erosion rates is a crucial for the assessment of the potential future environmental problems and land degradation in the TP (Wang et al., 2014).

Thus, our aims here are to address both of these challenges: first, to predict the present soil erosion by water on the TP using RUSLE, second, to predict the rainfall erosivity factor value in the 2050s with climate projections from six CMIP5 Global climate models (GCMs), and third to estimate the soil erosion by water in the 2050s with the corresponding projected rainfall erosivity. Our assumption here is that soil erosion by water in the TP is driven largely by climate.

2. Materials and methods

In this study, the current soil erosion by water was estimated with RUSLE, where the factors were derived from various point and remote sensing data sets. The current rainfall erosivity value was modelled by using a multiple linear regression (MLR) under current climate conditions. We generalised this model but using the future climate data from six GCMs to predict the rainfall erosivity value in the 2050s. The potential soil loss in the 2050s was then predicted by these rainfall erosivity and other erosion factors. We describe our approaches below.

2.1 RUSLE model

RUSLE is a linear equation used to quantify the soil loss potential via water from hillslopes (Kinnell, 2010). RUSLE is suitable for predicting long-term soil erosion rates over large areas according to the following equation:

$$A = R \times K \times LS \times C \times P \qquad (1)$$

where A is the average rate of soil erosion by water at each cell (t ha^{-1} y^{-1}); R is the rainfall erosivity factor (MJ mm ha^{-1} h^{-1} y^{-1}); K is the soil erodibility factor (t ha h ha^{-1} MJ^{-1} mm^{-1}); LS is the slope length and steepness factor; C is the cover management factor; and P is the support practice factor. We describe the derivation of the factors below.

The R factor is an indicator of the potential of precipitation to detach and transport soil particles. In this study, daily observed precipitation data that provided by the National Climate Centre of the China Meteorological Administration (CMA) and Tropical Rainfall Measuring Mission (TRMM) were used in our calculation of R. For the fifteen-year period from 2002–2016, 105 rain gauge stations were available across the TP (Figure 1). We used rainfall estimates from the TRMM 3B42 Version 7, which have a spatial resolution of 0.25°×0.25° and a temporal resolution of 3 h (Ma et al., 2017). The R factor was calculated following the approach presented in Teng et al., (2017). Collocated cokriging (ColCOK) was used to merge the daily rainfall data that from the rain gauge stations and TRMM measurements to improve the quality of the precipitation data. The merged daily rainfall data was then used to calculate R with a power function model, which was widely used in China and implemented by the National Water Conservancy Survey (Duan et al., 2016; Teng et al., 2017).

$$R_k = m \sum_{i=1}^{j} (d_i^j)^n \tag{2}$$

where R_k is the R value of the i half-month (MJ mm ha^{-1} h^{-1}); j is the number of days in the k half month; d_i^j is the effective precipitation for day i of the k half-month, which is no less than 12 mm for the ith day (Ma et al., 2014). Otherwise, d_i^j is equal to zero. The parameters m and n are defined as

$$m = 21.586 * n^{-7.1891} \tag{3}$$

$$n = 0.8363 + \frac{18.114}{d_{12}} + \frac{24.455}{y_{12}} \tag{4}$$

where d_{12} is the average daily rainfall (larger than 12 mm) and y_{12} is the yearly average rainfall for days with rainfall larger than 12 mm.

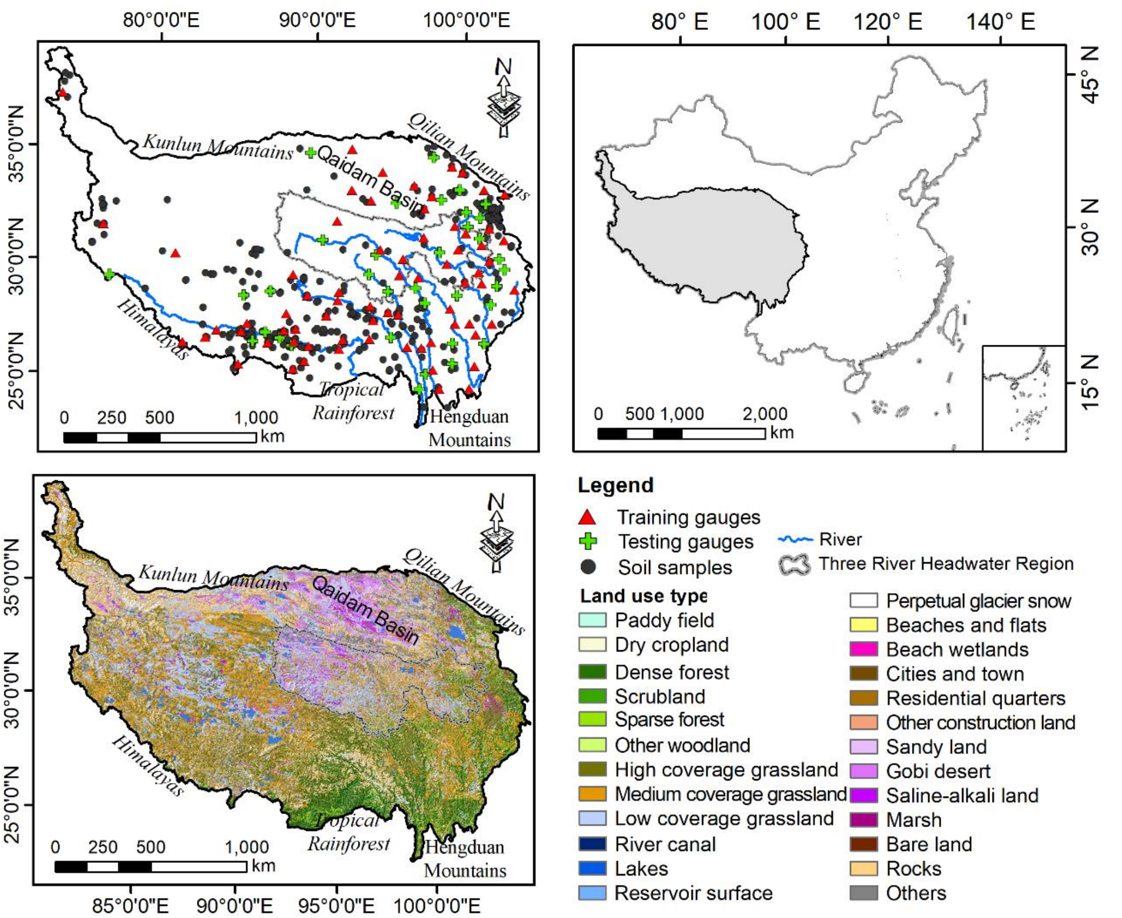

Figure 1. Location of rain gauges and soil samples used in this study across the Tibetan Plateau. The red triangles show the training rain gauges used to estimate annual rainfall erosivity. The green crosses represent testing rain gauge stations used to validate the result of annual rainfall erosivity. The black circles represent the locations for which soil samples were available to estimate soil erodibility.

Annual and monthly *R* was aggregated by *R* value of each half-month. In this case, the outcome of *R* factor was averaged to obtain the mean *R* from 2002 to 2016 at a 0.25°×0.25° resolution. We downscaled the *R* factor to 1 km spatial resolution with Random Forest (RF) (Breiman, 2001) using a set of environmental variables at 1 km resolution (see Table 1). RF has been successfully used elsewhere for spatial downscaling (He et al., 2016; Hutengs and Vohland, 2016; Ibarra-Berastegi et al., 2011). The 105 rain gauges were randomly separate into a training set (70) and a test set (35) (see Figure 1) before the application of ColCOK to obtain the merged daily rainfall data. The gauges in the test set were retained and used in an independent assessment of the performance of the model. The predictive performance of the *R* value was estimated by using the relevant statistical indices of the coefficient of determination (R^2) and root mean square error (RMSE).

Table 1. List of the auxiliary environmental predictors in the downscaling model of rainfall erosivity map and DSM model of soil erodibility map.

Factor	Environmental variables	Resolution	Source
Terrain	DEM	90 m	Shuttle Radar Topography Mission (SRTM)
	Slope	90 m	Shuttle Radar Topography Mission (SRTM)
	Aspect	90 m	Shuttle Radar Topography Mission (SRTM)
	Curvature	90 m	Shuttle Radar Topography Mission (SRTM)
	Roughness Index (TRI)	90 m	Shuttle Radar Topography Mission (SRTM)
	Topographic Wetness Index (TWI)	90 m	Shuttle Radar Topography Mission (SRTM)
	MrVBF	90 m	Shuttle Radar Topography Mission (SRTM)
Climate	Mean annual rainfall (Rain)	1 km	China Meterological Administration (CMA)
	Mean annual temperature (Temperature)	1 km	China Meterological Administration (CMA)
	Mean annual solar radiation (Radiation)	1 km	Data Center for Resources and Environmental Sciences, Chinese Academy of Sciences (RESDC)
	Mean annual evapotranspiration (ET)	1 km	Moderate-resolution imaging spectroradiometer (MODIS)
	Land Surface Temperature_day (LST_d)	1 km	Moderate-resolution imaging spectroradiometer (MODIS)
	Land Surface Temperature_night (LST_n)	1 km	Moderate-resolution imaging spectroradiometer (MODIS)
	Prescott Index (PI)	90 m	Shuttle Radar Topography Mission (SRTM)
Vegetation	NDVI	250 m	Moderate-resolution imaging spectroradiometer (MODIS)
	NPP	1 km	Moderate-resolution imaging spectroradiometer (MODIS)
Land/Soil	Land use type (LUCC)	1 km	Data Center for Resources and Environmental Sciences, Chinese Academy of Sciences (RESDC)
	Soil type	1 km	Data Center for Resources and Environmental Sciences, Chinese Academy of Sciences (RESDC)
	Sand	1 km	Harmonized World Soil Database (HWSD)
	Silt	1 km	Harmonized World Soil Database (HWSD)
	Clay	1 km	Harmonized World Soil Database (HWSD)
	TOC	1 km	Harmonized World Soil Database (HWSD)

The soil erodibility factor, *K*, can be estimated using soil texture and soil organic carbon data (Sharpley & Williams, 1990). In this study, these data were collected from the 410 soil profiles analysed during the Second National Soil Survey (NSSO, 1993, 1994a, 1994b, 1995a, 1995b, 1996, 1998). The locations of these data are shown in Figure 1. The *K* values at these points were calculated following recommendations of (Wischmeier and Smith, 1978). This model was also used in the National Soil and Water Conservation Survey of China.

$$K = 0.1317 * \left(0.2 + 0.3 * e^{\left[-0.0256 * San * \left(1 - \frac{Sil}{100}\right)\right]}\right) * \left(\frac{Sil}{Cla + Sil}\right)^{0.3} * \left[1 - \frac{0.25 * TOC}{TOC + e^{(3.72 - 2.95 * TOC)}}\right] * \left[1 - \frac{0.7 * SN_1}{SN_1 + e^{(22.9 * SN_1 - 5.51)}}\right] \quad (5)$$

where *San* is the sand content (0.05-2mm), %; *Sil* is the silt content (0.002-0.05mm), %; *Cla* is the clay content (<0.002mm), %; *TOC* is the soil total organic carbon content, %; and SN_1=1-*San*/100. After multiplied by 0.1317, the *K* value is expressed in SI metric (t ha h ha^{-1} MJ^{-1} mm^{-1}). In this model, the soil texture of international system was transformed into USDA system firstly using log-linear interpolation method.

The *K* values were mapped over the TP at 1 km resolution, using environmental factors that were listed in the Table 1 and digital soil mapping technique (McBratney et al., 2003). It should be noted that the environmental variables of sand, silt, clay and TOC in the Table 1 were not included in the *K* mapping. The method that we used, which is similar to that described in (Teng et al., 2016) and (Viscarra Rossel and Chen, 2011), is a Cubist regression model. From the 410 data, we selected at random 136 data for validation. The other 274 data was used for training the model, which we assessed by 10-fold cross validation. To assess its accuracy, the final model was evaluated by the independent validation data set and we reported the R^2 and RMSE of the predictions.

The *LS* factor represents the influence of slope length and slope gradient on soil loss. In this study, we calculated the *LS* factor using the 3 arc-second grid Shuttle Radar Topography Mission (SRTM) DEM following to the methodology described in Wischmeier and Smith (1978).

$$L = (a/22.13)^b \tag{6}$$

$$a = Flowaccumulation * cellsize \tag{7}$$

$$b = \frac{\beta}{(1+\beta)} \tag{8}$$

$$\beta = \frac{(sin\alpha/0.0896)}{[3*(sin\alpha)^{o.8} + 0.56]} \tag{9}$$

$$S = \begin{cases} 10.8sin\alpha + 0.03, & s < 9\% \\ 16.8sin\alpha - 0.5, & s \geq 9\% \end{cases} \tag{10}$$

where *a* is the slope length (m); *α* is the slope of DEM (%); and *s* is the slope gradient based on the slope of a standard RUSLE plot.

The cover management factor, *C*, estimates the effects of canopy cover, surface vegetation, surface roughness, prior land use, mulch cover and soil organic material on the erosion (Mhangara et al., 2012). These factors are difficult and costly to measure over the whole TP and have great variability during the growing season. The support practice factor, *P*, which reflect the effect of contouring and tillage practices (Wischmeier and Smith, 1978), can be estimated based on land use according to the land cover type. In this study, *C* and *P* factors are derived from the best available land cover type for analysing the land cover over the TP, China's 1 km resolution Land-Use/Cover Data set (CLUD), which is provided by the Data Centre for Resources and Environmental Sciences at the Chinese Academy of Sciences (RESDC) (http://www.resdc.cn). *C* and *P* factor values derived from former studies were used to reclassify the CLUD (Table 2).

Table 2. The *C* and *P* factor values of different land use type in the Tibetan Plateau.

Land use type	C value	Reference	P value	Reference
Paddy fields	0.1	Dai et al., 2013; Li et al., 2013; Yang et al., 2003	0.01	Lu et al., 2013; Dai et al., 2013
Dry cropland	0.22	Dai et al., 2013	0.4	Xu et al., 2013; Chen and Zha, 2016
Dense forest	0.006	Li et al., 2013	1	Xu et al., 2013; Dai et al., 2013
Scrubland	0.22	Fu et al., 2005; Du et al., 2016	1	Xu et al., 2013; Dai et al., 2013
Sparse forest	0.02	Li et al., 2013	1	Xu et al., 2013; Dai et al., 2013
Other woodland	0.44	Liu et al., 2015	0.7	Zhang, et al. 2016; Dai et al., 2013
High coverage grassland	0.08	Yang et al., 2003	1	Zhang, et al. 2016
Median coverage grassland	0.2	Yang et al., 2003	1	Zhang, et al. 2016
Low coverage grassland	0.25	Yang et al., 2003	1	Zhang, et al. 2016
Sandy land	0.35	Yang et al., 2003	1	Sun et al., 2014
Gobi desert	0.35	Yang et al., 2003	1	Sun et al., 2014
Saline-alkali land	0.35	Yang et al., 2003	1	Sun et al., 2014
Marsh	0.05	Yang et al., 2003	1	Xu et al., 2013
Bare soil	0.35	Yang et al., 2003	1	Zhang, et al. 2016; Dai et al., 2013
Bare rock	0.35	Yang et al., 2003	1	Sun et al., 2014
Other unused land	0.35	Yang et al., 2003	1	Xu et al., 2013

Having estimated all of the factors needed for the RUSLE (Eq. 1), we proceeded to calculate the current (2002–2016) soil erosion by water on the TP.

2.2 Comparison of current erosion with other assessments

The current estimates of soil erosion by water was compared to those derived by (Yue et al., 2016), who based his estimates on the Second National Soil Erosion Survey of China and included topographical, land use and remote-sensing inputs in addition to field survey data. The Second National Soil Erosion Survey reported soil erosion grades: Slight, Light, Moderate, Intense, Extremely Intense, and Severe, according to the Technological Standard of Soil and Water Conservation (SL190-2007), which was issued by the Ministry of Water Resources of China (Table 3). They did not use erosion rates because of the uncertainties in the input data and the model they used (Yue et al., 2016). To compare our results, the estimated mean soil erosion by water in the TP was converted into six erosion grades according to Table 3. For each of the erosion grades (except for the Slight grade) in Table 3, the areas affected by soil erosion were calculated and then compared with those of (Yue et al., 2016).

Table 3. Conversion from soil erosion rate from erosion grade, with corresponding areas of each erosion grade and its proportion in the Tibetan Plateau. The standard of soil erosion classification was built by the Ministry of Water Resources of China (SL190-2007).

Soil loss modules ($t\ ha^{-1}\ yr^{-1}$)	Erosion grade	Area ($\times 10^4\ km^2$)	Ratio (%)
< 10	Grade 1 (Slight)	203.58	84.56

10-25	Grade 2 (Light)	18.82	7.82
25-50	Grade 3 (Moderate)	8.81	3.66
50-80	Grade 4 (Intense)	4.04	1.68
80-150	Grade 5 (Extremely Intense)	3.69	1.53
> 150	Grade 6 (Severe)	1.81	0.75

2.3 Spatial modelling and future prediction of soil erosion

We developed a multiple linear regression (MLR) between our current *R* value and a set of the climate, terrain and soil variables (Table 4), obtained from the WorldClim Data Portal (Hijmans et al., 2005), the Shuttle Radar Topography Mission (SRTM) (Jarvis et al., 2008) and the Harmonized World Soil Database (HWSD, FAO/IIASA/ISRIC/ISSCAS/JRC, 2012), respectively. The WorldClim Data Portal provides a set of global-gridded bioclimatic variables with a spatial resolution of 1 km. There are 19 variables derived from monthly temperature and rainfall that represent annual trends, seasonality and extreme or limiting environmental factors (Hijmans et al., 2005).

The dataset (Table 4) used in the MLR was randomly separated into training and validation sets. Two-thirds of the dataset were assigned to the training set, and the remainder were assigned to the test set. Additionally, the performance of different spatial models was assessed by 10-fold cross validations and the boot-strap out-of-bag samples on the training set. The final model, which produced the best statistics, was used to predict the independent test. The performance of the model that was finally used in this study was assessed by statistical indexes of R^2, RMSE, ME and MSE.

Table 4. List of the auxiliary environmental predictors in the multiple linear regression model.

Base model (B) /projection model (P)	Factor	Predictors	Resolution	Source
BP	Terrain	DEM (m)	90 m	SRTM
		Slope (deg)	90 m	SRTM
		Aspect (deg)	90 m	SRTM
B	Climate (current)	Bio-climatic parameters [a]	1 km	WorldClim
P	Climate (2050)	Bio-climatic parameters [a]	1 km	WorldClim
BP	Soil	Sand (%)	1 km	HWSD
		Silt (%)	1 km	HWSD
		Clay (%)	1 km	HWSD
		TOC	1 km	HWSD

[a] Climate data derivatives (WorldClim BioClimatic Parameters, Current and 2050): annual mean temperature (bio1), mean diurnal range (mean of monthly (max temp−min temp)) (bio2), isothermality (bio3), temperature seasonality (standard deviation ∗ 100) (bio4), max temperature of warmest month (bio5), minimum temperature of coldest month (bio6), temperature annual range (bio7), mean temperature of wettest quarter (bio8), mean temperature of driest quarter (bio9), mean temperature of warmest quarter (bio10), mean temperature of coldest quarter (bio11), annual precipitation (bio12), precipitation of wettest month (bio13), precipitation of driest month (bio14), precipitation seasonality (coefficient of variation) (bio15), precipitation of wettest quarter (bio16), precipitation of driest quarter (bio17), precipitation of warmest quarter (bio18), and

precipitation of coldest quarter (bio19).

In this study, a stepwise regression algorithm was employed to prevent overfitting the data and to find the optimal regression model. The MLR coefficients were multiplied with climate variables derived from the GCMs scenarios for the year 2050 to produce future estimates of *R* factor. The residuals of the MLR were added to these predictions to obtain our estimates of the *R* factor in 2050 in the TP at 1 km resolution. Outputs of 19 bioclimatic variables from six GCMs (Table 5) in the CMIP5 are used to represent future climate factors. Two extreme representative concentration pathways (RCP); RCP2.6 and RCP8.5 (Taylor et al., 2009) were used for investigating the climate projections over the TP. The GCM-derived bioclimatic variables were downscaled and calibrated with WorldClim 1.4 by (Hijmans et al., 2005). We obtained them from the WorldClim Data Portal (http://www.worldclim.org/). The final estimates of potential soil loss in 2050 was derived by using predicted *R* factor in 2050 and other erosion factors (*K*, *LS*, *C*, and *P*) which are considered indirectly affect by climate change in this study.

Table 5. Summary of the six GCMs from CMIP5.

Model name	Institution	Country	Resolution (Longitude×Latitude)
BCC-CSM1.1	Beijing Climate Center, China Meteorological Administration	China	~2.8125°× 2.8125°
GFDL-CM3	Geophysical Fluid Dynamics Laboratory	United States	2.5°×2°
IPSL-CM5A-LR	L'Institut Pierre-Simon Laplace	France	3.75°× ~1.9°
MIROC-ESM	Japan Agency for Marine-Earth Science and Technology, Atmosphere and Ocean Research Institute (The University of Tokyo), and National Institute for Environmental Studies	Japan	~2.8°× 2.8°
MPI-ESM-LR	Max Planck Institute for Meteorology (MPI-M)	Germany	1.875°× ~1.9°
NorESM1-M	Norwegian Climate Centre	Norway	2.5°× ~1.9°

3. Results

3.1 Current rate of soil erosion by water

Maps of the RUSLE factors on the TP are shown in Figure 2. Areas without soil (cities, rocks, water bodies, permanent glaciers and salt crusts) were masked from the maps and were not included in the results.

The predicted map of the annual *R* factor on the TP at 1 km spatial resolution is shown in Figure 2a. The validation R^2 and RMSE for the downscaled *R* factor in the RK model were 0.88 and 841.39 MJ mm ha^{-1} h^{-1} y^{-1}, respectively. The mean annual *R* on the TP value was 309 MJ mm ha^{-1} h^{-1} y^{-1}. The smallest values of *R* (< 10 MJ mm ha^{-1} h^{-1} y^{-1}) were mostly observed in the northern part of the TP. The highest *R* value (> 2000 MJ mm ha^{-1} h^{-1} y^{-1}) was observed in the south of the TP, which is consistent with the subtropical monsoon and humid climate in this region. Our calculation of *R* compared well to the 35 testing rain gauges data, with $R^2 = 0.81$ and RMSE = 293.15 MJ mm ha^{-1} h^{-1} y^{-1}.

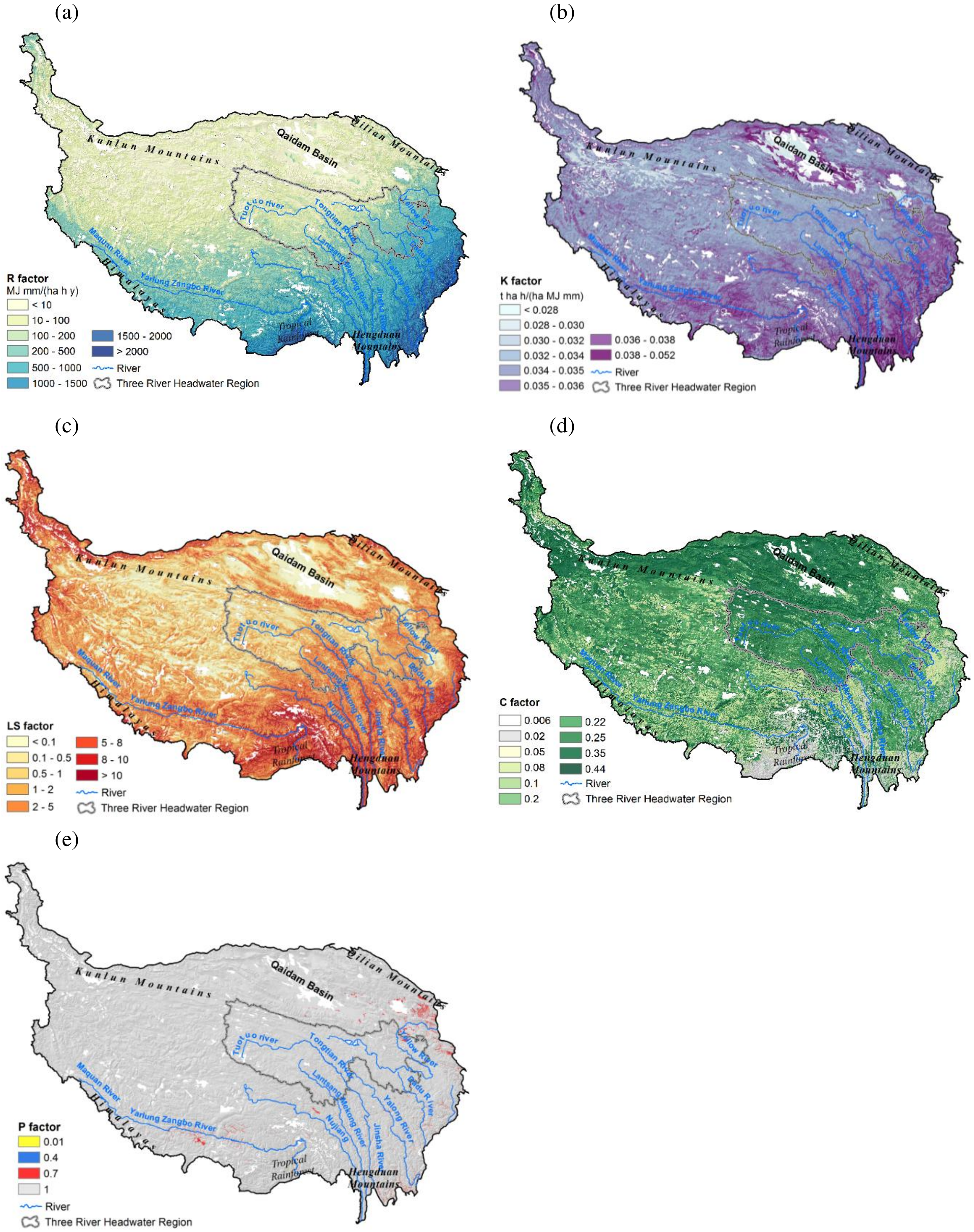

Figure 2. Maps at a 1 km resolution of: (a) rainfall erosivity, *R* factor, (b) soil erodibility, *K* factor, (c) slope length and steepness, *LS* factor, (d) cover management, *C* factor, and (e) support practice, *P* factor.

The K factor map is shown in Figure 2b. The validation R^2 and RMSE for the K map were 0.58 and 0.047 t ha h ha^{-1} MJ^{-1} mm^{-1}, respectively. The mean K value of the TP was 0.034 t ha h ha^{-1} MJ^{-1} mm^{-1}. Figure 2b shows that the least erodible soils (K values less than 0.030 t ha h ha^{-1} MJ^{-1} mm^{-1}) are found mostly in the low-lying desert regions with sandy soil, soil rich in calcium carbonate, soil with a cemented layer known as caliche (typically in the Qaidam Basin) and consolidated Pedocal soil, which are not easily detached and transported by overland flow. The most erodible soils (K values in the range from 0.038 to 0.052 t ha h ha^{-1} MJ^{-1} mm^{-1}) were found mostly in forests or mixed vegetative cover areas, and sites in the southern and eastern TP. Alfisols and Semi-Alfisols (the Chinese Genetic Soil Classification, Shi et al., 2004) had the largest K values (Figure 2b).

Figure 2c shows the LS factor map. On the TP, the mean LS factor value was 3.13. The lowest value of LS factor (< 0.1) occurred in the lowest areas of the Qaidam Basin, while highest value of LS factor (> 10) occurred in the Hengduan Mountains and southern Himalayas. Figure 2c shows that the large LS values were consistent with high topographies and coincided with escarpments in the Himalayas and Hengduan Mountains, which rendered these areas extremely susceptible to erosion.

The C factor map is shown in Figure 2d. The largest values of C occurred in the Qaidam Basin in areas with no vegetation cover, whereas the smallest C values occurred in evergreen broad-leaved forests within the rain forests of the southern slopes of the eastern Himalayas and tropical rainforest areas. The Kunlun Mountains, which are mainly covered by low coverage grassland and bare rocks, and the cultivated land in the valley regions of the southern TP, had relatively large C values. The west areas of the Plateau, which are mainly covered by shrubs and steppe, had moderate C values.

P-factor map is shown in Figure 2e, it reflects the reduction in soil erosion caused by anthropomorphic impacts. On the TP, human engineering activities are limited and primarily focus on farmland, which mainly occurred in the valley regions of the tropical forest areas, and on other woodland, especially on all kinds of garden areas.

The resulting RUSLE map of the annual rate of soil erosion by water on the TP is shown in Figure 3a. On the TP, the average hillslope soil loss was 8.34 t ha^{-1} y^{-1}, and the TP presented a potential annual soil loss of approximately 1,604×10^6 tonnes (Table 6). Areas in the south and east of the Plateau showed to have the greatest erosion. Smaller rates (< 1 t ha^{-1} y^{-1}) were evident in the centre and northern TP, particularly in the Qaidam Basin and southern Kunlun Mountains (Figure 3a).

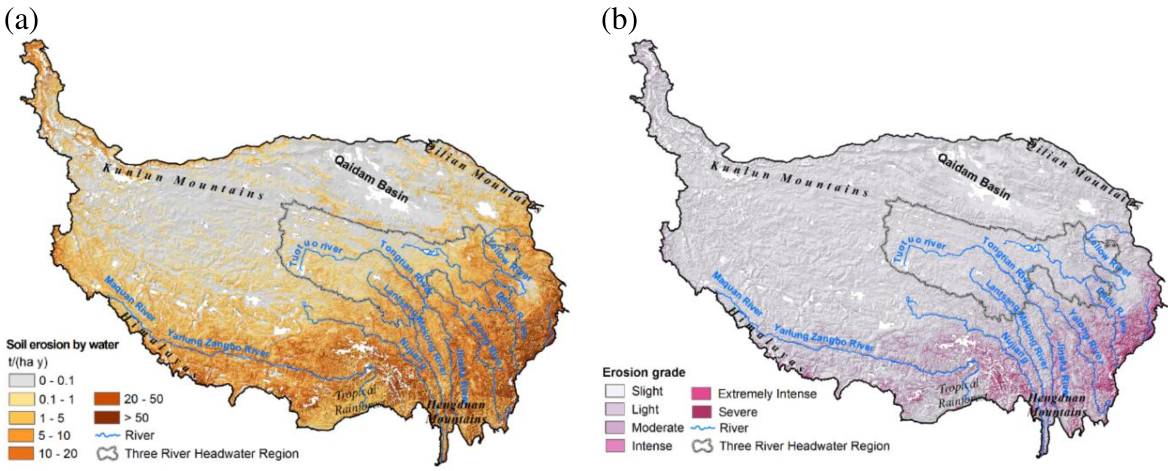

Figure 3. Maps of (a) predicted current (2002–2016) annual soil erosion by water and (b) soil erosion grade at 1 km resolution in the Tibetan Plateau.

Other woodlands, including young afforested land, slash and all kinds of garden, have the largest rate of erosion, but because of their limited areas in the TP they have experience relatively little total soil loss. Scrublands, which are mainly occurred in the areas of strong vertical zonality, have a relatively large erosion rate. Crop lands, including paddy fields and dry cropland, have erosion rates larger than the average value for the whole TP. The total erosion on the grasslands occupy 60% of the total erosion on the TP. The smallest average annual soil loss occurs on marsh, sandy, desert and saline-alkali lands (Table 8)

Table 3 shows that erosion grade 1 (Slight) areas account for the largest proportion of the total erosional area and primarily occur in the central and northern TP, whereas erosion grade 6 (Severe) areas account for the lowest proportion of the total erosional area on the TP and primarily occur in the Hengduan Mountains and the border areas of eastern TP (Figure 3b).

3.2 Comparing soil loss estimates with other assessments

Figure 4 presents a map of the areas that were influenced by water erosion at different erosion grades on the TP and shows a comparison between our results and those of Yue et al. (2016). Compared to the estimates made by Yue et al. (2016), we obtained larger estimates in the Light and Moderate erosion grades of counties in the southern Plateau, and smaller estimates in counties of the north-eastern Plateau (Figure 4). In the regions of Extremely Intense and Severe erosion, there weren't marked differences between our estimates of erosion areas and those of Yue et al. (2016), although our estimates were larger in regions of the south-eastern TP.

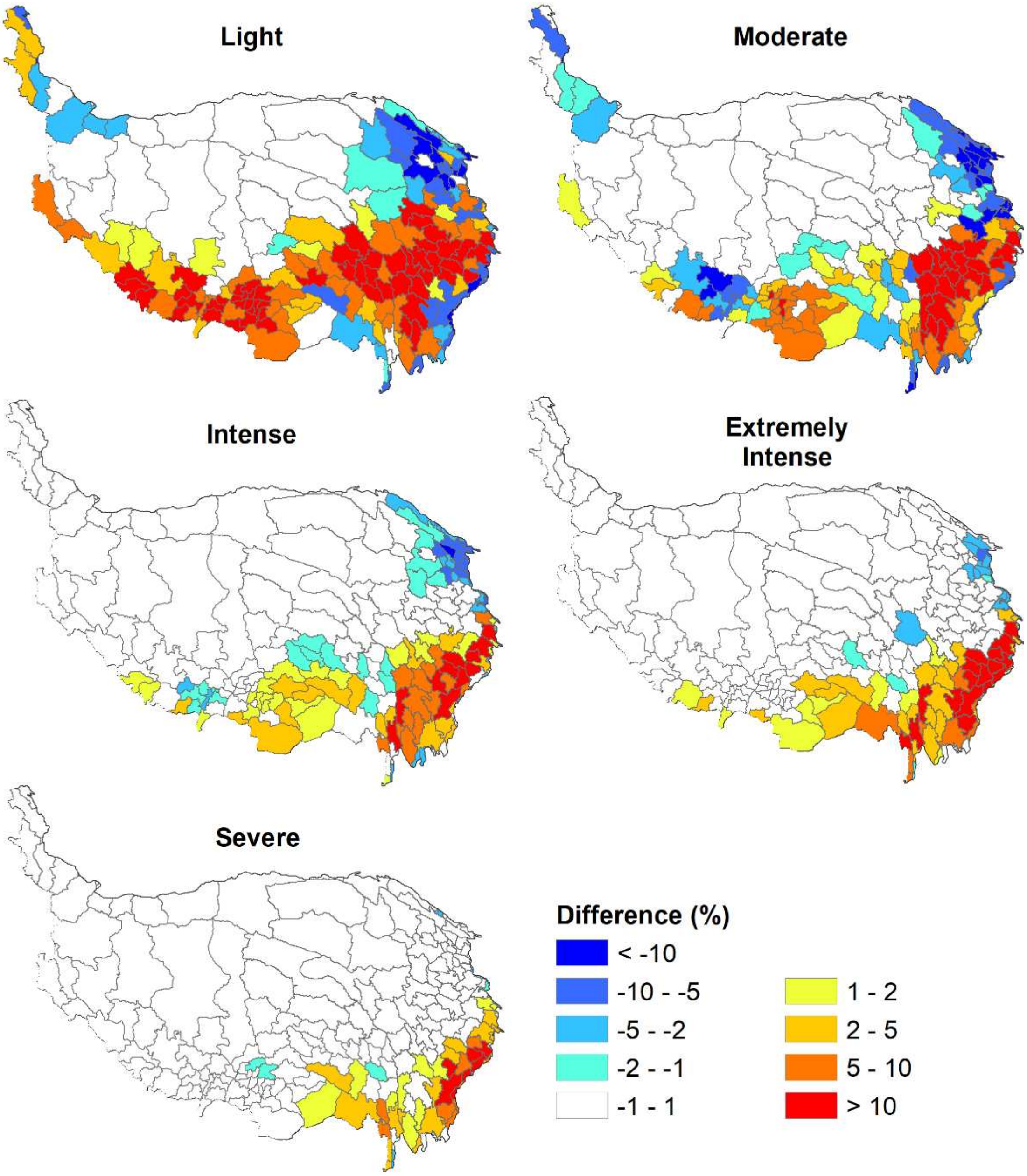

Figure 4. Difference maps between this study and second national soil erosion survey of China based on the erosion grade in the Tibetan Plateau. Red means larger estimate in this study, blue means smaller estimate in this study.

3.3 Projected future soil loss potential on the Tibetan Plateau

The parameters of the MLR are given in Table 6. In this section, stepwise regression was used to fit regression model and choose predictive variables. With stepwise regression analysis the factor, temperature annual range (bio7), which had little influence on the *R* factor was excluded. Table 7 shows the validation statistics of the MLR modelling. The assessment statistics from the predictions of the test data set were close to those from the 10-fold cross validations and the OOB statistics. The results suggested that the MLR model that we built was robust and accurate (R^2 > 0.85 for each of the validation). Figure 5a shows the residual map of the MLR model. The Moran's I value of the residual map is 0.88 and indicate that the residual of the MLR model has an obviously spatial autocorrelation. The variogram of the residual map is shown in Figure 5b.

Table 6. The results of the stepwise multiple linear regression model. Note that the stepwise regression was used to fit regression model and choose predictive variables.

Coefficients	Estimate	Std.Error	t value	Signif. Codes	Coefficients	Estimate	Std.Error	t value	Signif. Codes
Intercept	-1765.00	11.77	-149.96	***	bio8	-0.05	0.02	-3.48	***
DEM	-0.06	0.00	-104.61	***	bio9	0.22	0.01	22.54	***
Slope	1.81	0.01	148.93	***	bio10	49.98	0.18	271.40	***
Clay	1.98	0.02	101.41	***	bio11	-66.48	0.18	-364.38	***
Sand	0.34	0.01	39.97	***	bio12	3.80	0.01	490.83	***
Silt	0.19	0.01	14.71	***	bio13	16.36	0.04	412.55	***
toc	-4.97	0.08	-61.70	***	bio14	82.88	0.20	407.59	***
bio1	12.93	0.10	133.48	***	bio15	1.03	0.01	71.77	***
bio2	-26.45	0.08	-320.49	***	bio16	-12.37	0.04	-335.06	***
bio3	91.71	0.26	347.44	***	bio17	-32.07	0.11	-284.24	***
bio4	-1.83	0.00	-443.81	***	bio18	0.81	0.03	28.52	***
bio5	14.99	0.07	226.30	***	bio19	1.26	0.05	27.69	***
bio6	-12.05	0.05	-244.05	***					

Significance codes: ***<0.001

Table 7. 10-fold cross validation, out-of-bag (OOB) and independent test set validation statistics for the multiple linear regression model. Assessment with the coefficient of determination (R^2), the root mean square error (RMSE), the mean error (ME), and the mean squared error (MSE).

	R^2	RMSE	ME	MSE
Cross validation statistics	0.859	164.08	-0.02	26715.18
Out of bag statistics	0.857	164.55	-0.16	27076.74
Test set statistics	0.857	164.08	-0.02	26922.92

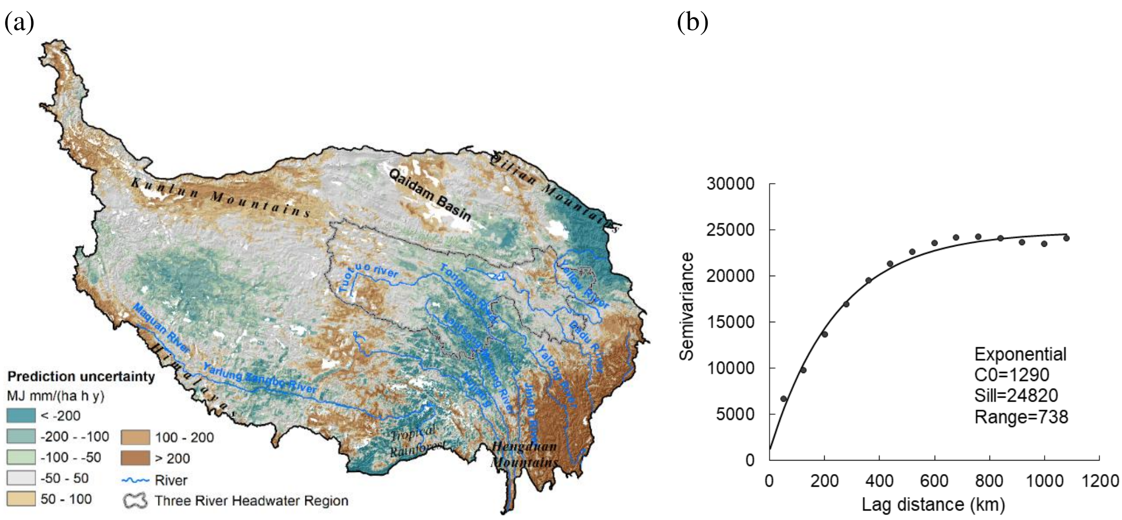

Figure 5. Maps of (a) residual of the MLR model, and (b) its semi-variogram.

The maps of the projected *R* factor and the corresponding potential soil erosion by water in 2050 according to six GCMs and two RCPs are shown in Figures 6a and 6b. Figure 6a shows that high *R* value in 2050 mainly occur in the southeast tropical rainforest areas and the southeast border areas. Figure 6b shows that soil erosion will mainly occur in the south part of the TP. Figure 7a shows the major differences of *R* factor in 2050 between six GCMs and two RCPs occur in the middle and southwest part of the Plateau. *R* factor in 2050 predicted by climate scenarios of MIROC-ESM and NorESM1-M showed increase in the middle part of the Plateau, whereas that predicted by climate scenarios of IPSL-CM5A-LR showed a decreasing tendency in most of these areas (Figure 7a). *R* factor in 2050 predicted by climate scenarios of GFDL-CM3 and MIROC-ESM showed decrease in the southwestern TP, while with climate scenarios of IPSL-CM5A-LR and MPI-ESM-LR an increasing tendency was observed in most of these areas (Figure 7a). From our estimates, erosion in the southeast tropical rainforest areas of the Plateau will increase in 2050 by climate scenarios of BCC-CSM1.1, GFDL-CM3, and IPSL-CM5A-LR by RCP2.6 and RCP8.5, whereas estimates using climate scenarios of MIROC-ESM and NorESM1-M by RCP2.6 and RCP8.5 show overall decrease in 2050 in these areas (Figure 7b). The estimates of the soil erosion remain stable in 2050 over the most of the middle areas of the Plateau according to the six GCMs and two RCPs (Figure 7b).

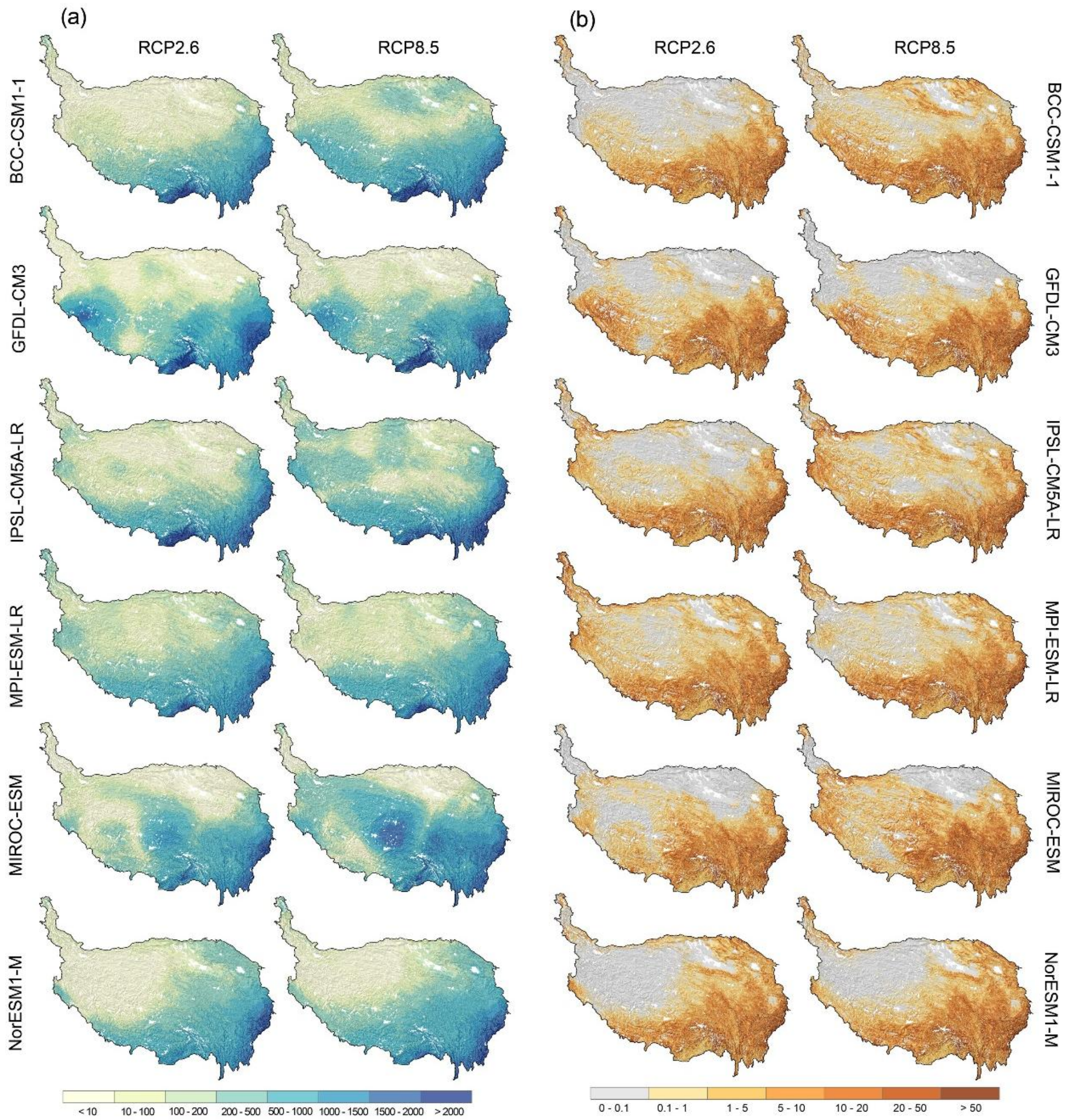

Figure 6. (a) Maps of rainfall erosivity factor by 2050 by Climate Scenarios and Representative Concentration Pathways (RCPs). First row: BCC-CSM1-1(RCP2.6, 8.5). Second row: GFDL-CM3 (RCP2.6, 8.5). Third row: HadGEM2-AO (RCP2.6, 8.5). Fourth row: IPSL-CM5A-LR (RCP2.6, 8.5). Fifth row: MPI-ESM-LR (RCP2.6, 8.5). Sixth row: MIROC-ESM (RCP2.6, 8.5). (b) Maps of potential soil loss by 2050 by Climate Scenarios and Representative Concentration Pathways (RCPs). First row: BCC-CSM1-1(RCP2.6, 8.5). Second row: GFDL-CM3 (RCP2.6, 8.5). Third row: HadGEM2-AO (RCP2.6, 8.5). Fourth row: IPSL-CM5A-LR (RCP2.6, 8.5). Fifth row: MPI-ESM-LR (RCP2.6, 8.5). Sixth row: MIROC-ESM (RCP2.6, 8.5). Units of (a) MJ mm ha^{-1} h^{-1} y^{-1}, and (b) t ha^{-1} y^{-1}.

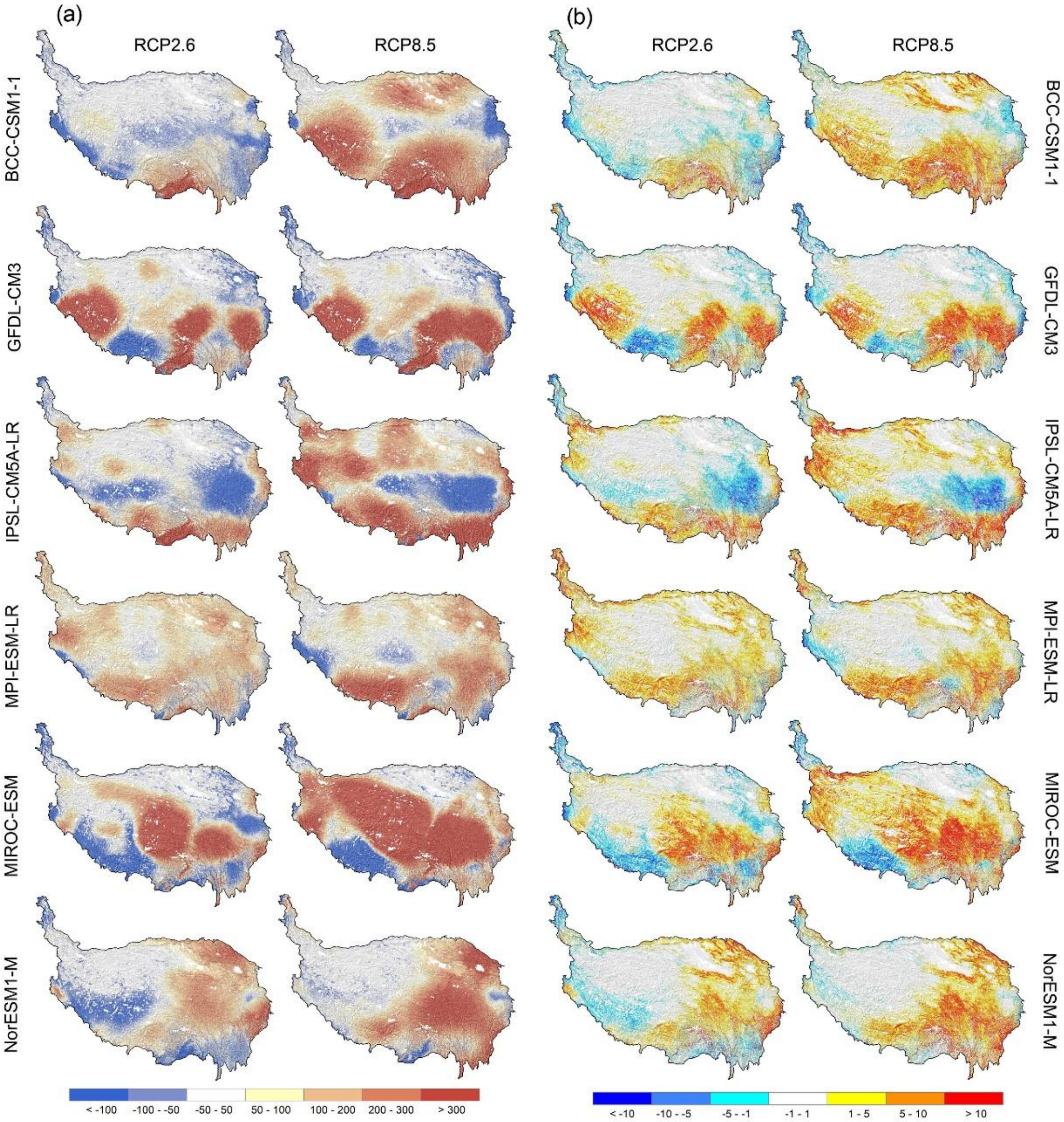

Figure 7. (a) Change of rainfall erosivity factor by 2050 by Climate Scenarios and Representative Concentration Pathways (RCPs). First row: BCC-CSM1-1(RCP2.6, 8.5). Second row: GFDL-CM3 (RCP2.6, 8.5). Third row: HadGEM2-AO (RCP2.6, 8.5). Fourth row: IPSL-CM5A-LR (RCP2.6, 8.5). Fifth row: MPI-ESM-LR (RCP2.6, 8.5). Sixth row: MIROC-ESM (RCP2.6, 8.5). Blue areas represent decrease and red areas represent increase in rainfall erosivity value (MJ mm ha^{-1} h^{-1} y^{-1}) compared to current value. (b) Change of potential soil loss by 2050 by Climate Scenarios and Representative Concentration Pathways (RCPs). First row: BCC-CSM1-1(RCP2.6, 8.5). Second row: GFDL-CM3 (RCP2.6, 8.5). Third row: HadGEM2-AO (RCP2.6, 8.5). Fourth row: IPSL-CM5A-LR (RCP2.6, 8.5). Fifth row: MPI-ESM-LR (RCP2.6, 8.5). Sixth row: MIROC-ESM (RCP2.6, 8.5). Blue areas represent decrease and red areas represent increase in potential soil loss (t ha^{-1} y^{-1}) compared to current value.

Table 8 lists the estimated current mean and total soil loss (with standard deviations) on the Tibetan Plateau and our 2050 predictions for different land uses. The estimation in 2050 was the value that averaged by six GCMs. The average projected potential soil erosion by water, which based on the six GCMs, of the TP in 2050 according to the RCP2.6 and RCP8.5 was 9.73 and 11.60 t ha^{-1} y^{-1}, respectively. The TP presented a potential annual soil loss of approximately 1,825×10^6 and 2,148×10^6 tonnes in 2050, respectively. Other unused land and gobi desert showed largest relative change of soil erosion rates in 2050 according to RCP2.6 and RCP8.5, while other woodland and scrubland showed the smallest relative change of mean soil erosion rates (Table 8).

Table 8. Estimates of annual potential soil loss in the Tibetan Plateau by land use type in current and 2050. (Units: t $ha^{-1}y^{-1}$; $t\times10^{6}$ y^{-1})

Land use	Description	Current			RCP2.6(2050)				RCP8.5(2050)			
		Mean	SD	Total	Mean	SD	Total	Relative change	Mean	SD	Total	Relative change
Other woodland	Young afforested land, slash, all kinds of garden	55.90	83.25	6.62	56.17	80.80	6.65	0.48	63.04	90.15	7.47	12.76
Scrubland	Scrubland with a crown density > 40% and height less than 2 m	45.23	77.38	416.41	48.43	82.21	447.73	7.09	53.32	90.22	493.01	17.88
Paddy fields	flooded parcel of arable land used for growing semiaquatic rice	20.09	35.61	0.04	22.37	39.60	0.05	11.36	21.66	38.46	0.05	7.82
Dry cropland	Rainfed cropland without water supply and irrigating facilities	13.87	21.76	21.69	14.93	23.58	23.54	7.66	16.10	25.20	25.57	16.10
Sparse forest	Woodland with a crown density of 10%–30%	12.88	34.56	29.87	13.95	38.08	32.51	8.35	15.25	42.90	35.54	18.41
Dense forest	Woodland with a crown density > 30%	11.19	38.02	165.14	12.10	42.07	180.60	8.20	13.21	46.37	197.27	18.12
Median coverage grassland	Grassland with a coverage between 20% and 50%	9.25	27.04	510.50	10.40	29.72	574.75	12.41	12.27	32.44	677.90	32.57
High coverage grassland	Grassland with a coverage > 50%	6.38	19.0	264.17	7.38	22.00	306.26	15.67	8.85	25.08	367.15	38.65

Low coverage grassland	Natural grassland with a coverage of 5%–20%	3.47	15.36	174.06	4.35	17.48	218.17	25.15	5.76	20.48	289.27	65.90
Other unused land	Other unused land, including Alpine deserts and tundra.	1.32	5.25	10.44	3.28	7.75	25.86	147.61	5.09	9.92	40.16	284.53
Marsh	Land with accumulated water and hygrocolous plants	0.65	4.58	1.27	0.82	4.97	1.60	26.21	1.01	6.32	2.00	57.10
Sandy land	Land covered with sand, vegetation coverage < 5%	0.37	2.97	1.60	0.50	3.61	2.18	36.07	0.74	4.58	3.23	102.00
Gobi desert	Stony and alpine deserts with a vegetation coverage < 5%	0.22	1.06	2.11	0.50	1.69	4.80	127.91	0.89	2.57	8.54	305.51
Saline-alkali land	Land with more salt gathered on top soil	0.14	0.91	0.40	0.23	1.49	0.66	65.38	0.41	2.19	1.15	187.41
TP	The Tibetan Plateau	8.34	31.37	1604.33	9.73	34.64	1825.36	16.65	11.60	38.67	2148.31	39.13

*Relative change = ($Mean_{2050}$-$Mean_{current}$)/ $Mean_{current}$ *100

4. Discussion

Soil erosion on the TP is complicated and diverse, it includes water erosion, freezing-thaw erosion, wind erosion, etc. Some studies have assessed soil erosion on TP, especially for the wind erosion (Han et al., 2014; Rohrmann et al., 2013; Xie et al., 2017; Yan et al., 2005; Yan et al., 2001; Zhang et al., 2007a) and freezing-thaw erosion (Guo et al., 2017; Guo et al., 2015; Yi et al., 2013; Zhang et al., 2007b). However, as a remote area that is sensitive to climate variability, the water erosion on the whole TP has been rarely reported quantitatively, and none of them has predicted future soil erosion risk on the TP. The work that we present here on the assessment and future prediction of soil erosion by water is timely because changing climatic conditions can potentially increase the risk of soil and land degradation on the TP (Wang et al., 2017), which can also affect its unique biodiversity and ecology.

In this study, the soil erosion by water on the TP is based on the RUSLE. Our estimates of soil erosion by water on the TP will show more accuracy than those derived in previous assessments, not only because the new data source that we used to compute erosion factors, but also because the improved methodologies were incorporated into the calculation. The *R* factor in this study was calculated based on the merged daily rainfall data with rigorously quality control. Teng et al., (2017) demonstrated that the improved estimates of the *R* factor showed higher accuracy than the simple interpolated gauge-based approach. The *K* factor that we modelled in this study was based on the comprehensive soil properties and environment data sets currently available and geospatial methods.

According to our result, land that is under forest have experienced relatively high erosion rates. However, this result showed inconsistency with other researchers. (Garcia-Ruiz et al., 2015) undertook a meta-analysis of published soil erosion data from more than 4000 sites worldwide and showed that forests have relatively low erosion rates. (Panagos et al., 2015) estimated soil loss by water in Europe for the reference year of 2010 and found that forests have the lowest rate of soil loss. This inconsistency between our results and other studies can attribute to the specific geographical characteristics in the TP. Forest in the TP mainly distribute in the areas with precipitation more than 400 mm (Zhao et al., 2015). These areas mainly occur in the southern TP with high elevation and steepness. Thus, forest in these areas usually have high *R* and *LS* value, and explain the high rate of soil erosion.

Compared to Yue et al. (2016), who assessed erosion for the whole of China based on the Second National Soil Erosion Survey, our estimates are continuous and at 1-km resolution, were made using modern geospatial modelling, using the best available data and specifically for the TP. The difference between our study and Yue et al., (2016) might be related to the different data source in the erosion factors estimation, especially to the *R* and *K* factors. The *R* value in the Yue et al., (2016) was obtained using interpolation of the calculated *R* value on the rain gauge stations that provided by the CMA. The accuracy of their estimates of *R* will depend on the spatial density of the interpolated rain gauges. However, these stations are unevenly distributed on the TP and very few are located in the southeast tropical rainforest areas. It may be for this reason that they estimated less erosion in the southeast areas of the Plateau. Our *R* factor map was also derived using data from the CMA. However, our estimates of *R* are likely to be better because we first merged rainfall data from the rain gauges and the TRMM satellite, and then downscaled *R* to produce estimates that are specific for the TP. The southeast tropical rainforest areas are influenced by the monsoon climate and have the highest amount of rainfall in the Plateau. A local study in southeast tropical rainforest areas conducted by Fan et al.

(2013) confirmed the larger R values and reported that it is around 12,189 MJ mm ha^{-1} h^{-1} yr^{-1}, which is similar to our results.

Liu et al., (2014) calculated the K values of all the soil types on the TP based on the soil profile data and GIS. According to Liu et al., (2014), the K value on the TP range from 0.026 t ha h ha^{-1} MJ^{-1} mm^{-1} to 0.039 t ha h ha^{-1} MJ^{-1} mm^{-1}, with a mean value of 0.03 t ha h ha^{-1} MJ^{-1} mm^{-1}. The highest value of K factor in the Liu et al., (2014) occurred in the northeast of Qinghai Province, while the lowest value of K factor occurred in the Qaidam Basin. All these results are similar to ours. Our results also consist with Wang et al., (2004). Wang et al., (2004) showed that the southeast Tibet is more erodible than the northwest Tibet. Most areas of the TP have a relatively small value of K.

Downscaling methods have been employed in former studies to assess the impact of climate change on soil erosion (Li and Fang, 2016). Among them, regression models, which have the characteristics of low computation requirements and ease of implementation, can be regarded as the most popular methods. In this study, MLR was used to calculate future R factor by testing the relationship between current R values and environmental factors, and to project them into 2050 by using the same regression coefficients. The soil erosion risk in 2050 was then predicted by the changing R factor in 2050. The approach in this study is similar to that used by Yigini and Panagos (2016), and it assumes that erosion, especially erosion factor of rainfall erosivity, is largely governed by climate.

The future soil erosion prediction for the TP, using six models with respect to the regional climate, indicate that the southwest TP appears to be an area that is most at risk of erosion by 2050, especially if the conditions of scenario RCP8.5 occur, which corresponding to the pathway with the largest climate variability and highest greenhouse gas emissions. This area is largely affected by the westerlies and monsoon with large precipitation occurring in the wet season. (Su et al., 2016) suggested that this area is more likely to experience future temperature increases compared to other regions in the TP. Changes in runoff across this area are closely linked to temperature and precipitation increases. The increasing trend of soil total runoff for this area under the scenario of RCP2.6 and RCP8.5 indicating the future erosion risk in 2050. The occurrence of increased soil erosion by water may influence local ecosystems in the TP and hence induce hydrologic variations in the rivers originating from the Plateau, such as the Yangtze River, the Yellow River and the Lantsang-Mekong River.

There are some limitations to our approach, and there are also sources of uncertainty influence our results. The *C* factors in this study are related to the land use type. Conventionally, *C* factor is calculated as a product of canopy cover, canopy height, residual cover, below-ground biomass and time. However, these factors are difficult to measure for the whole TP. The method that we used in this study to measure *C* factor might not be fully capable of illustrating the content of the *C* factor, and might induce some uncertainty of our results. There are some uncertainties occurred in the procedures of the *R* downscaling and *K* mapping. These uncertainties will remain in the following calculation of soil erosion by water. We used two emissions scenarios for future projections that falls on the lowest and highest end of all warming scenarios. However, how much warming will actually occur on the TP still uncertain. The results of soil erosion that predicted by the six GCMs provide different trends in some regions of the TP, this reflect the high uncertainty of predicted future soil erosion. The six GCMs and two scenarios that we used here was attempted to avoid a larger part of the model bias. We believe the scenarios and projection models that we used provided a useful soil erosion threshold in 2050.

5. Conclusions

The TP was demonstrated to be a sensitive area corresponding to climate change. Quantifying the impacts of climate change and its effect on soil erosion over the TP is important to assist policy-makers and land managers in adopting strategies for its protection and conservation. However, limited observations of water erosion in the TP have been reported quantitatively.

This study produced the best estimates of current (2002–2016) erosion in the TP by RUSLE based on the most current and available data sets. Improved methodologies were applied to calculate the erosion factors of *R* and *K*. A MLR model was built between the current *R* value and sets of the climate, terrain and soil variables to predict *R* factor value and erosion in the year 2050.

We found the average soil erosion by water on the TP is 8.34 t ha^{-1} y^{-1}, which equates to potential annual soil losses of $1,604\times10^{6}$ tonnes over this area. Areas that suffer from severe soil erosion occur in the Hengduan Mountains and the southeastern Himalayas. Land that is under other woodland and scrubland have the highest erosion rate. Our estimates of current erosion are comparable to those made by other researchers.

Our predicted of soil erosion in 2050 suggests an increase under the six future climate models and two RCPs. The average projected potential soil erosion by water of the TP in 2050 according to the RCP2.6 and RCP8.5 was 9.73 and 11.60 t ha^{-1} y^{-1}, respectively, which equates to potential annual soil losses of $1,825\times10^{6}$ tonnes and $2,148\times10^{6}$ tonnes, respectively, over the TP. Water and soil conservation measures over the TP should be continued and strengthened. The southeast tropical rainforest areas and areas with high slopes and high altitudes are more sensitive to climate variability; therefore, the increased risk of soil erosion over these areas should be further studied.

The methods that we used in this study were useful for characterization of soil erosion by water over large areas. As it can process data input for large regions with sparse data, RUSLE can provide quantitative estimates of long-term soil erosion by water in the TP. The method that we used, which incorporated regression model, climate models and scenarios, can provide a threshold of future soil erosion rates in 2050 with low bias.

Acknowledgements

This study is supported by National Natural Science Foundation of China (No. 41461063, 41571339, 41661061), and the Fundamental Research Funds for the Central Universities Zhejiang. Raphael A. Viscarra Rossel thanks the High-end Foreign Experts Recruitment Program.

References

Amundson, R., Berhe, A.A., Hopmans, J.W., Olson, C., Sztein, A.E., Sparks, D.L., 2015. Soil and human security in the 21st century. Science 348(6235).

Baumann, F., He, J.S., Schmidt, K., Kuhn, P., Scholten, T., 2009. Pedogenesis, permafrost, and soil moisture as controlling factors for soil nitrogen and carbon contents across the Tibetan Plateau. Global Change Biol 15(12), 3001-3017.

Breiman, L., 2001. Random Forests. Machine Learning 45(1), 5-32 http://link.springer.com/article/10.1023/A%3A1010933404324.

Chaplot, V.A.M., Rumpel, C., Valentin, C., 2005. Water erosion impact on soil and carbon redistributions within uplands of Mekong River. Global Biogeochem Cy 19(4).

Chappell, A., Baldock, J., Sanderman, J., 2016. The global significance of omitting soil erosion from soil organic carbon cycling schemes. Nat Clim Change 6(2), 187-191.

Chen, H., Zhu, Q.A., Peng, C.H., Wu, N., Wang, Y.F., Fang, X.Q., et al., 2013. The impacts of climate change and human activities on biogeochemical cycles on the Qinghai-Tibetan Plateau. Global Change Biol 19(10), 2940-2955.

Chen, S.F., Zha, X., 2016. Evaluation of soil erosion vulnerability in the Zhuxi watershed, Fujian Province, China. Nat Hazards 82(3), 1589-1607.

Dai, Z.H., Feng, X.B., Zhang, C., Shang, L.H., Qiu, G.L., 2013. Assessment of mercury erosion by surface water in Wanshan mercury mining area. Environ Res 125, 2-11.

Du, H.Q., Dou, S.T., Deng, X.H., Xue, X., Wang, T., 2016. Assessment of wind and water erosion risk in the watershed of the Ningxia-Inner Mongolia Reach of the Yellow River, China. Ecol Indic 67, 117-131.

Du, M.Y., Kawashima, S., Yonemura, S., Zhang, X.Z., Chen, S.B., 2004. Mutual influence between human activities and climate change in the Tibetan Plateau during recent years. Global Planet Change 41(3-4), 241-249.

Duan, X.W., Gu, Z.J., Li, Y.G., Xu, H.J., 2016. The spatiotemporal patterns of rainfall erosivity in Yunnan Province, southwest China: An analysis of empirical orthogonal functions. Global Planet Change 144, 82-93.

Fan, J.R., Chen, Y., Yan, D., Guo, F.F., 2013. Characteristics of rainfall erosivity based on tropical rainfall measuring mission data in Tibet, China. J Mt Sci-Engl 10(6), 1008-1017.

FAO/IIASA/ISRIC/ISSCAS/JRC, 2012. Harmonized World Soil Database (Version 1.2). FAO and IIASA, Rome and Laxenburg.

Fu, B.J., Zhao, W.W., Chen, L.D., Zhang, Q.J., Lu, Y.H., Gulinck, H., et al., 2005. Assessment of soil erosion at large watershed scale using RUSLE and GIS: A case study in the Loess Plateau of China. Land Degrad Dev 16(1), 73-85.

Garcia-Fayos, P., Bochet, E., 2009. Indication of antagonistic interaction between climate change and erosion on plant species richness and soil properties in semiarid Mediterranean ecosystems. Global Change Biol 15(2), 306-318.

Garcia-Ruiz, J.M., Begueria, S., Nadal-Romero, E., Gonzalez-Hidalgo, J.C., Lana-Renault, N., Sanjuan, Y., 2015. A meta-analysis of soil erosion rates across the world. Geomorphology 239, 160-173.

Guo, B., Luo, W., Wang, D.L., Jiang, L., 2017. Spatial and temporal change patterns of freeze-thaw erosion in the three-river source region under the stress of climate warming. J Mt Sci-Engl 14(6), 1086-1099.

Guo, B., Zhou, Y., Zhu, J.F., Liu, W.L., Wang, F.T., Wang, L.T., et al., 2015. An estimation method of soil freeze-thaw erosion in the Qinghai-Tibet Plateau. Nat Hazards 78(3), 1843-1857.

Han, W.X., Ma, Z.B., Lai, Z.P., Appel, E., Fang, X.M., Yu, L.P., 2014. Wind erosion on the north-eastern Tibetan Plateau: constraints from OSL and U-Th dating of playa salt crust in the Qaidam Basin. Earth Surf Proc Land 39(6), 779-789.

He, X.G., Chaney, N.W., Schleiss, M., Sheffield, J., 2016. Spatial downscaling of precipitation using adaptable random forests. Water Resour Res 52(10), 8217-8237.

Hijmans, R.J., Cameron, S.E., Parra, J.L., Jones, P.G., Jarvis, A., 2005. Very high resolution interpolated climate surfaces for global land areas. Int J Climatol 25(15), 1965-1978.

Hren, M.T., Chamberlain, C.P., Hilley, G.E., Blisniuk, P.M., Bookhagen, B., 2007. Major ion chemistry of the Yarlung Tsangpo-Brahmaputra river: Chemical weathering, erosion, and CO2 consumption in the southern Tibetan plateau and eastern syntaxis of the Himalaya. Geochim Cosmochim Ac 71(12), 2907-2935.

Hutengs, C., Vohland, M., 2016. Downscaling land surface temperatures at regional scales with random forest regression. Remote Sens Environ 178, 127-141.

Ibarra-Berastegi, G., Saenz, J., Ezcurra, A., Elias, A., Argandona, J.D., Errasti, I., 2011. Downscaling of surface moisture flux and precipitation in the Ebro Valley (Spain) using analogues and analogues followed by random forests and multiple linear regression. Hydrol Earth Syst Sc 15(6), 1895-1907.

IPCC (Intergovernmental Panel on Climate Change), 2014. Climate Change 2014: Impacts, Adaptation, and Vulnerability. Contribution of Working Group II to the Fifth Assessment Report of the Intergovernmental Panel on Climate Change. Cambridge University Press: Cambridge, UK.

Immerzeel, W.W., van Beek, L.P.H., Bierkens, M.F.P., 2010. Climate Change Will Affect the Asian Water Towers. Science 328(5984), 1382-1385.

Jarvis, A., Reuter, H.I., Nelson, A., Guevara, E.. 2008. Hole-filled SRTM for the globe Version 4.

available from the CGIAR-CSI SRTM 90m Database (http://srtm. csi. cgiar. org).

Jiang, C., Zhang, L.B., 2016. Ecosystem change assessment in the Three-river Headwater Region, China: Patterns, causes, and implications. Ecol Eng 93, 24-36.

Karydas, C.G., Panagos, P., Gitas, I.Z., 2014. A classification of water erosion models according to their geospatial characteristics. Int J Digit Earth 7(3), 229-250.

Kinnell, P.I.A., 2010. Event soil loss, runoff and the Universal Soil Loss Equation family of models: A review. J Hydrol 385(1-4), 384-397.

Li, X.S., Wu, B.F., Zhang, L., 2013. Dynamic monitoring of soil erosion for upper stream of Miyun Reservoir in the last 30 years. J Mt Sci-Engl 10(5), 801-811.

Li, Z.Y., Fang, H.Y., 2016. Impacts of climate change on water erosion: A review. Earth-Sci Rev 163, 94-117.

Liu, B.T., Tao, H.P., Shi, Z., Song, C.F., Guo, B., 2014. Spatial Distribution Characteristics of Soil Erodibility K Value in Qinghai-Tibet Plateau. Bull. Soil Water Conserv 34, 11-16. (in Chinese)

Liu, Y.S., Guo, Y.J., Li, Y.R., Li, Y.H., 2015. GIS-based effect assessment of soil erosion before and after gully land consolidation: A case study of Wangjiagou project region, Loess Plateau. Chinese Geogr Sci 25(2), 137-146.

Lu, Q.S., Xu, B., Liang, F.Y., Gao, Z.Q., Ning, J.C., 2013. Influences of the Grain-for-Green project on grain security in southern China. Ecol Indic 34, 616-622.

Ma, X., He, Y., Xu, J., van Noordwijk, M., Lu, X., 2014. Spatial and temporal variation in rainfall erosivity in a Himalayan watershed. Catena 121, 248-259

Ma, Z.Q., Shi, Z., Zhou, Y., Xu, J.F., Yu, W., Yang, Y.Y., 2017. A spatial data mining algorithm for downscaling TMPA 3B43 V7 data over the Qinghai-Tibet Plateau with the effects of systematic anomalies removed. Remote Sens Environ 200, 378-395.

McBratney, A.B., Santos, M.L.M., Minasny, B., 2003. On digital soil mapping. Geoderma 117(1-2), 3-52.

Mhangara, P., Kakembo, V., Lim, K.J., 2012. Soil erosion risk assessment of the Keiskamma catchment, South Africa using GIS and remote sensing. Environ Earth Sci 65(7), 2087-2102.

National Soil Survey Office (NSSO). 1993. Soil Species of China, (Vol. 1). Chinese Agricultural Press: Beijing. (in Chinese).

National Soil Survey Office (NSSO). 1994a. Soil Species of China, (Vol. 2). Chinese Agricultural Press: Beijing. (in Chinese).

National Soil Survey Office (NSSO). 1994b. Soil Species of China, (Vol. 3). Chinese Agricultural Press: Beijing. (in Chinese).

National Soil Survey Office (NSSO). 1995a. Soil Species of China, (Vol. 4). Chinese Agricultural Press: Beijing. (in Chinese).

National Soil Survey Office (NSSO). 1995b. Soil Species of China, (Vol. 5). Chinese Agricultural Press: Beijing. (in Chinese).

National Soil Survey Office (NSSO). 1996. Soil Species of China, (Vol. 6). Chinese Agricultural Press: Beijing. (in Chinese).

National Soil Survey Office (NSSO). 1998. Soils of China. Chinese Agricultural Press: Beijing. (in Chinese).

Navarro-Hevia, J., Lima-Farias, T.R., de Araujo, J.C., Osorio-Pelaez, C., Pando, V., 2016. Soil Erosion in Steep Road Cut Slopes in Palencia (Spain). Land Degrad Dev 27(2), 190-199.

Pan, B.T., Geng, H.P., Hu, X.F., Sun, R.H., Wang, C., 2010. The topographic controls on the decadal-scale erosion rates in Qilian Shan Mountains, NW China. Earth Planet Sc Lett 292(1-2), 148-157.

Panagos, P., Borrelli, P., Poesen, J., Ballabio, C., Lugato, E., Meusburger, K., et al., 2015. The new assessment of soil loss by water erosion in Europe. Environ Sci Policy 54, 438-447.

Qiu, J., 2008. The third pole. Nature 454(7203), 393-396.

Renard, K.G., Foster, G.R., Weesies, G.A., McCool, D.K., Yoder, D.C. 1997. Predicting soil erosion by water: a guide to conservation planning with the Revised Universal Soil Loss Equation (RUSLE). 703. United States Department of Agriculture, Washington, DC.

Rohrmann, A., Heermance, R., Kapp, P., Cai, F.L., 2013. Wind as the primary driver of erosion in the Qaidam Basin, China. Earth Planet Sc Lett 374, 1-10.

Sharpley, A.N., Williams, J.R., 1990. EPIC–Erosion/Productivity Impact Calculator: 1. Model Documentation. Washington, DC: USDA Technical Bulletin No. 1768.

Shi, X.Z., Yu, D.S., Warner, E.D., Pan, X.Z., Petersen, G.W., Gong, Z.G., Weindorf, D.C., 2004. Soil database of 1:1,000,000 digital soil survey and seference system of the Chinese Genetic Soil Classification System. Soil Horizons 45, 129-136.

Su, F., Zhang, L., Ou, T., Chen, D., Yao, T., Tong, K., et al., 2016. Hydrological response to future climate changes for the major upstream river basins in the Tibetan Plateau. Global Planet Change 136, 82-95.

Su, F.G., Duan, X.L., Chen, D.L., Hao, Z.C., Cuo, L., 2013. Evaluation of the Global Climate Models in the CMIP5 over the Tibetan Plateau. J Climate 26(10), 3187-3208.

Sun, W.Y., Shao, Q.Q., Liu, J.Y., Zhai, J., 2014. Assessing the effects of land use and topography on soil erosion on the Loess Plateau in China. Catena 121, 151-163.

Taylor, K.E., Stouffer, R.J., Meehl, G.A., 2009. A summary of the CMIP5 experimental design. Accessed on 6 April 2010. available from: http://cmip-pcmdi.llnl.gov/cmip5/experiment design.html.

Teng, H.F., Viscarra Rossel, A.V., Shi, Z., Behrens, T., Chappell, A., Bui, E., 2016. Assimilating satellite imagery and visible-near infrared spectroscopy to model and map soil loss by water erosion in Australia. Environ Modell Softw 77, 156-167.

Teng, H.T., Ma, Z.Q., Chappell, A., Shi, Z., Liang, Z.Z., Yu, W., 2017. Improving Rainfall Erosivity Estimates Using Merged TRMM and Gauge Data. Remote Sens 9, 1134.

Viscarra Rossel, R.A., Chen, C., 2011. Digitally mapping the information content of visible-near infrared spectra of surficial Australian soils. Remote Sens Environ 115(6), 1443-1455.

Wang, Y.S., Cheng, C.C., Xie, Y., Liu, B.Y., Yin, S.Q., Liu, Y.N., et al., 2017. Increasing trends in rainfall-runoff erosivity in the Source Region of the Three Rivers, 1961-2012. Sci Total Environ 592, 639-648.

Wang, X.D., Zhong, X.H., Fan, J.R., 2004. Assessment and spatial distribution of sensitivity of soil erosion in Tibet. J. Geogr. Sci. 14, 41–46.

Wang, Y.Z., Zhang, H.P., Zheng, D.W., Zheng, W.J., Zhang, Z.Q., Wang, W.T., et al., 2014. Controls on decadal erosion rates in Qilian Shan: Re-evaluation and new insights into landscape evolution in north-east Tibet. Geomorphology 223, 117-128.

Wischmeier, W.H., Smith, D.D., 1978. Predicting Rainfall Erosion Losses: A Guide to

Conservation Planning. US Department of Agriculture.

Xie, S.B., Qu, J.J., Xu, X.T., Pang, Y.J., 2017. Interactions between freeze-thaw actions, wind erosion desertification, and permafrost in the Qinghai-Tibet Plateau. Nat Hazards 85(2), 829-850.

Xu, L.F., Xu, X.G., Meng, X.W., 2013. Risk assessment of soil erosion in different rainfall scenarios by RUSLE model coupled with Information Diffusion Model: A case study of Bohai Rim, China. Catena 100, 74-82.

Xu, X.L., Liu, W., Kong, Y.P., Zhang, K.L., Yu, B.F., Chen, J.D., 2009. Runoff and water erosion on road side-slopes: Effects of rainfall characteristics and slope length. Transport Res D-Tr E 14(7), 497-501.

Yan, H., Wang, S.Q., Wang, C.Y., Zhang, G.P., Patel, N., 2005. Losses of soil organic carbon under wind erosion in China. Global Change Biol 11(5), 828-840.

Yan, P., Dong, Z.B., Dong, G.R., Zhang, X.B., Zhang, Y.Y., 2001. Preliminary results of using Cs-137 to study wind erosion in the Qinghai-Tibet Plateau. J Arid Environ 47(4), 443-452.

Yang, D.W., Kanae, S., Oki, T., Koike, T., Musiake, K., 2003. Global potential soil erosion with reference to land use and climate changes. Hydrol Process 17(14), 2913-2928.

Yi, S., Li, N., Xiang, B., Wang, X., Ye, B., McGuire, A.D., 2013. Representing the effects of alpine grassland vegetation cover on the simulation of soil thermal dynamics by ecosystem models applied to the Qinghai-Tibetan Plateau. J Geophys Res-Biogeo 118(3), 1186-1199.

Yigini, Y., Panagos, P., 2016. Assessment of soil organic carbon stocks under future climate and land cover changes in Europe. Sci Total Environ 557, 838-850.

Yue, Y., Ni, J.R., Ciais, P., Piao, S.L., Wang, T., Huang, M.T., et al., 2016. Lateral transport of soil carbon and land-atmosphere CO2 flux induced by water erosion in China. P Natl Acad Sci USA 113(24), 6617-6622.

Zhang, C.L., Zou, X.Y., Yang, P., Dong, Y.X., Li, S., Wei, X.H., et al., 2007a. Wind tunnel test and Cs-137 tracing study on wind erosion of several soils in Tibet. Soil Till Res 94(2), 269-282.

Zhang, J.G., Liu, S.Z., Yang, S.Q., 2007b. The classification and assessment of freeze-thaw erosion in Tibet. J Geogr Sci 17(2), 165-174.

Zhang, L., Bai, K.Z., Wang, M.J., Karthikeyan, R., 2016. Basin-scale spatial soil erosion variability: Pingshuo opencast mine site in Shanxi Province, Loess Plateau of China. Nat Hazards 80(2), 1213-1230.

Zhao, Y., Herzschuh, U., Li, Q., 2015. Complex vegetation responses to climate change on the Tibetan Plateau: a paleoecological perspective. Natl Sci Rev 2(4), 400-402.